Full reciprocal-space mapping up to 2000 K under controlled atmosphere: the multipurpose QMAX furnace

René Guinebretière, Stephan Arnaud, Nils Blanc, Nathalie Boudet, Elsa Thune, David Babonneau, Olivier Castelnau

Full reciprocal-space mapping up to 2000 K under controlled atmosphere: the multipurpose QMAX furnace

René Guinebretière,[a]* Stephan Arnaud,[b] Nils Blanc,[b] Nathalie Boudet,[b] Elsa Thune,[a] David Babonneau[c] and Olivier Castelnau[d]

[a]Université de Limoges, IRCER, UMR 7315, CNRS, Centre Européen de la Céramique, F-87068 Limoges, France, [b]Université Grenoble Alpes, CNRS, Institut Néel UPR CNRS 2940, 38000 Grenoble, France, [c]Université de Poitiers, Institut Pprime, Département Physique et Mécanique des Matériaux, UPR CNRS 3346, SP2MI, TSA 41123, 86073 Poitiers Cedex 9, France, and [d]Laboratoire PIMM, UMR CNRS 8006, ENSAM, CNAM, 151 Boulevard de l'Hôpital, 75013 Paris, France. *Correspondence e-mail: rene.guinebretiere@unilim.fr

Keywords: reciprocal-space mapping; high temperature; *in situ*; structural and microstructural evolution under extreme conditions; controlled atmosphere.

A furnace that covers the temperature range from room temperature up to 2000 K has been designed, built and implemented on the D2AM beamline at the ESRF. The QMAX furnace is devoted to the full exploration of the reciprocal hemispace located above the sample surface. It is well suited for symmetric and asymmetric 3D reciprocal space mapping. Owing to the hemispherical design of the furnace, 3D grazing-incidence small- and wide-angle scattering and diffraction measurements are possible. Inert and reactive experiments can be performed at atmospheric pressure under controlled gas flux. It is demonstrated that the QMAX furnace allows monitoring of structural phase transitions as well as microstructural evolution at the nanoscale, such as self-organization processes, crystal growth and strain relaxation. A time-resolved *in situ* oxidation experiment illustrates the capability to probe the high-temperature reactivity of materials.

1. Introduction

One of the current issues in materials science is to be able to determine *in situ* the structural and microstructural evolution of materials as a function of external constraints (Tao & Salmeron, 2011; Villanova *et al.*, 2017). X-ray scattering (diffuse scattering, small-angle X-ray scattering, diffraction) and absorption (tomography, absorption spectroscopy) experiments are nondestructive and very well suited for the characterization of actual materials during their elaboration or in operating conditions. However, dynamical experimental studies able to show on a convenient timescale the *in situ* evolution of materials under very high temperature or pressure, mechanical constraints, or environmental atmosphere variations through gas flows require the use of high-flux X-ray sources. It is well known that third-generation synchrotron radiation sources are very useful facilities in this field (Montano & Oyanagi, 1999). Nowadays, the combination of such X-ray sources and 2D position-sensitive detectors allows the collection of scattering or diffraction patterns in a second or even shorter timescales (Basolo *et al.*, 2007; Bergamaschi *et al.*, 2010; Örs *et al.*, 2018), and full 3D exploration of the reciprocal space can be achieved around any reciprocal lattice node (RLN) within an hour (Cornelius *et al.*, 2012) or less (Leake *et al.*, 2019). For many years, the structural or microstructural evolution (*i.e.* phase transitions, thermal expansion,

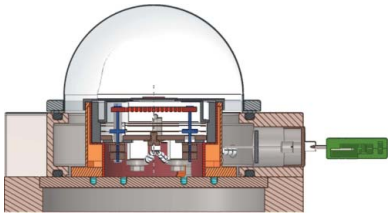

grain growth, defect mobility *etc.*) as a function of temperature or pressure has been studied through *in situ* X-ray-scattering-based methods. However, in many cases, the samples have to be prepared in such a way that they fit the experimental constraints related to the use of high-temperature furnaces or diamond-anvil cells. Consequently, the characterized samples are often very different, especially from the microstructural point of view, from the actual materials under consideration. It is thus an ongoing endeavor to develop X-ray scattering setups well suited to capturing the structural evolution of single-crystal surfaces, thin films, nanostructures and 3D bulk polycrystalline materials under reactive or nonreactive atmosphere at temperatures higher than 1250 K with a convenient timescale resolution.

Chemists who synthesize new compounds or develop crystal chemistry studies commonly realize high-temperature X-ray diffraction (XRD) experiments. In most cases, such studies are done on powdered samples, often put into capillary sample holders. The use of such capillary sample holders under the Debye–Scherrer diffraction geometry (Guinebretière, 2007) together with one-dimensional position-sensitive gaseous (Bénard *et al.*, 1996; Muller *et al.*, 1997) or solid-state (Pickup *et al.*, 2000; Sarin *et al.*, 2009) curved detectors allows high-angular-resolution diffraction patterns to be collected in a short time at temperatures as high as 1250 K. Nevertheless, such an approach is far from the characterization of single-crystal surfaces, thin films or bulk materials. On the other hand, cylindrical furnaces where platinum foil strips act simultaneously as heating element and sample holder have been under development for many years (Koppelhuber-Bitschnau *et al.*, 1996). However, a quite large expansion of these metallic strips and subsequent sample displacement are induced by the temperature increase. Although such setups have been widely used, accurate sample positioning as a function of temperature is still a difficult task (Brown *et al.*, 1993; Misture *et al.*, 2002; Beck & Mittemeijer, 2002), and sample displacement with respect to the goniometer axes has a large influence on the accuracy of the *d*-spacing measurements (Masson *et al.*, 1996). This drawback can be overcome by using cylindrical furnaces in which the samples are put on top of an alumina disc located on a spinning stage that corresponds to azimuthal rotation around the sample surface (Gualtieri *et al.*, 1999; Estermann *et al.*, 1999; Guinebretière *et al.*, 2007). Heating of the samples is usually realized using conventional high-temperature heaters located around the sample holder. Combination of this setup with a translational stage along the azimuthal φ rotation axis allows one to continuously compensate the sample holder thermal expansion (Gualtieri *et al.*, 1999; Guinebretière *et al.*, 2007). One of the most significant achievements using this configuration is certainly the furnace built by Yashima *et al.* (2006) on the 4B2 beamline at the Photon Factory in Japan. They demonstrated that the combination of such a cylindrical furnace and a multiple detector allows high-angular-resolution XRD patterns to be recorded at temperatures as high as 1900 K on a number of ceramic materials and the corresponding structures to be described (Yashima, 2002; Yashima & Tanaka, 2004).

The devices that we briefly described above are built in such a way that, whatever the detectors are, the X-rays scattered by the sample can be recorded only if they are scattered in the 'diffraction plane', *i.e.* the plane containing both the direction of the primary X-ray beam and the normal to the sample surface. Taking into account the limited width of the window of the cylindrical furnaces, very few X-ray beams scattered out of this plane can reach the detector. This is the main drawback of such setups, which has two different consequences: firstly, it strongly limits interest in the use of the 2D detectors that are nowadays increasingly used for 2D or 3D exploration of reciprocal space; secondly, it forbids in-plane measurements such as grazing-incidence small-angle X-ray scattering (GISAXS) or grazing-incidence diffraction (GID).

During the past few years, we have developed a new furnace allowing reciprocal space maps (RSMs) to be recorded up to 2000 K either close to the center of the reciprocal space, *i.e.* in the small-angle scattering regime, or around any diffraction nodes. We report here on the use of this setup, called the 'QMAX furnace', which we have implemented on the French Collaborating Research Group D2AM beamline at the ESRF (Chahine *et al.*, 2019). The QMAX furnace works in reflection mode and it allows GISAXS and GID to be collected as well as conventional out-of-plane diffraction patterns under symmetric or asymmetric configurations. Besides the very high temperatures that are under consideration, one of the main characteristics of the QMAX furnace is that the experiments are realized under controlled gas flux. *In situ* reactive experiments can thus easily be performed.

2. Description of the QMAX furnace

A global view of the QMAX furnace is provided in Fig. 1(*a*) and a cross-sectional drawing in Fig. 1(*b*). The implementation on the D2AM beamline goniometer is illustrated in Fig. 1(*c*). In order to be able to characterize bulk polycrystalline samples as well as thin films or single-crystal surfaces, the furnace has been designed for experiments in the reflection geometry under asymmetric incidence angles on flat samples (Guinebretière, 2007). The confinement of the atmosphere around the sample is realized using a hemispherical beryllium dome, and the furnace is designed such that the detector can collect all the X-rays scattered in the half-space above the sample. This geometry is similar to that chosen by the Anton Paar company for its 'DHS' heating stage series (Kotnik *et al.*, 2006). However, the maximal temperature accessible using those furnaces is, under optimal conditions, 1350 K, which is far below the accessible temperature with the QMAX furnace. Moreover, no accurate control of the gas flux is implemented on the DHS devices.

The heating of the samples is ensured by an 80Pt–20Rh plate put onto an alumina flat holder specifically designed so that it retains its integrity despite the differential expansion associated with temperature gradients. The way that the samples themselves are fixed onto the heating element depends on their nature (see below). Very near to the sample heating stage, a flowing-water cooling device made of two

coaxial copper cylinders allows the steel body of the furnace to be maintained at room temperature (RT). Additionally, an airflow shower located above the beryllium dome, *i.e.* above the entire furnace, allows keeping the temperature of the dome below 350 K to prevent the beryllium from oxidation whatever the temperature of the sample.

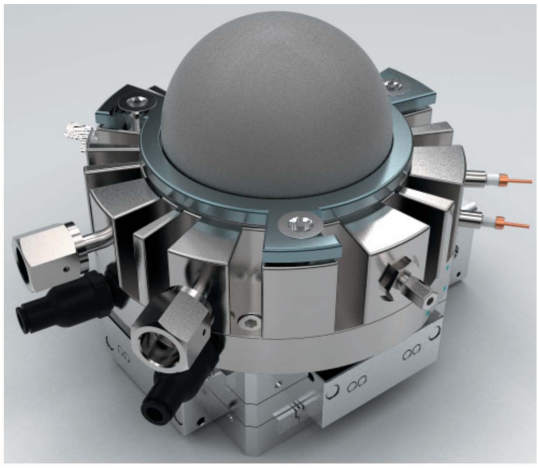

(*a*)

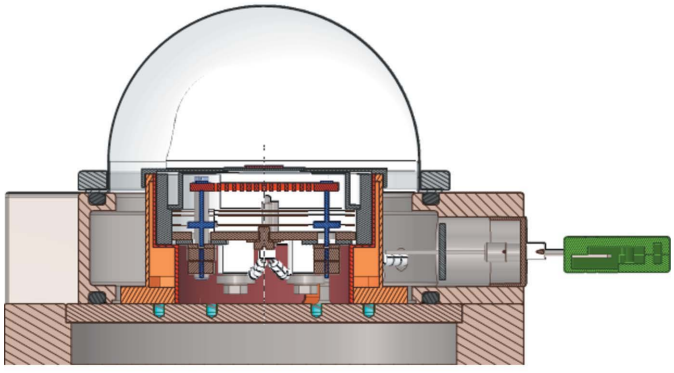

(*b*)

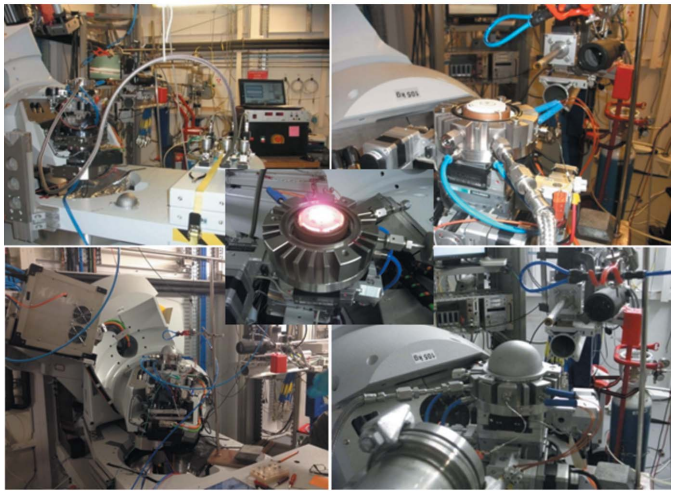

(*c*)

Figure 1
The QMAX furnace in its working environment at the D2AM beamline. (*a*) Photograph of the furnace, (*b*) cross-sectional drawing of the furnace, and (*c*) photographs showing the furnace at high temperature on the goniometer and all the associated devices.

The QMAX furnace internal temperature is measured using a Pt–10% Rh–Pt thermocouple located at roughly 1 mm underneath the sample. The temperature evolution is driven by a Nanodac controller from Eurotherm by Schneider Electric. It is linked to the computer driving the experimental setup and thus the temperature is recorded in a global data file. The proportional–integral–derivative furnace parameters can be fully controlled by the computer and adjusted as a function of the temperature. The heating rate can be as high as 50 K min^{-1}. The furnace itself is mounted above a motorized goniometer head made of two crossed cradles and two translations on top of the kappa stage of the D2AM goniometer (Chahine *et al.*, 2019). Throughout this article, the experiments will be described using the classical convention with respect to the goniometer rotation axis and reciprocal-space vector components (Guinebretière, 2007). The ω axis gives the incidence angle of the primary beam onto the sample surface, the φ axis is orthogonal to the ω axis and normal to a reference plane chosen by the experimentalist (the sample surface, any diffracting plane of a single crystal *etc.*), and the χ axis is orthogonal to the other two. After convenient positioning of the sample with respect to these goniometer axes using the motorized goniometer head, the q_x, q_y and q_z components of the scattering vectors are, respectively, collinear to the χ-axis, ω-axis and φ-axis unit vectors.

Using such a setup, flat samples placed in the furnace can be carefully aligned before X-ray scattering measurements at any temperature with respect to their surface or any of their diffracting planes with an angular accuracy of a few thousandths of a degree (Boulle *et al.*, 2001). Translational displacement of the samples due to thermal expansion can be fully compensated for using a z-translation stage situated below the goniometer head. After a first determination of the thermal expansion of the sample, an automatic compensation of this expansion can be implemented in the code driving the goniometer. Thus, whatever the temperature, the surface of the sample contains the cross point of the ω, φ and χ rotation axes of the diffractometer. This allows solution of the well known sample-displacement problem underlined by numerous authors (see above). As already said, the QMAX furnace is designed for the realization of experiments at atmospheric pressure under inert or reactive gas flow. Chemical reactions can be followed under a given gas or a mixture of two different gasses of any kind introduced into the furnace through computer-driven flowmeters allowing a gas flux of up to one litre per minute with a few millilitres per minute accuracy. The main technical characteristics of the QMAX furnace are given in Table 1.

One of the main characteristics of a furnace is of course the maximal temperature that can be reached during the experiment. Note that the temperature of interest is that of the sample and not the value of the temperature set-point. We performed a large number of experiments and we observed that the maximal accessible temperature depends on the nature of the samples and more specifically on their thermal properties, which themselves are related to the composition of the samples but also to their state (*i.e.* if it is a single crystal, a

Table 1
Main characteristics of the QMAX furnace.

Geometry of the X-ray scattering measurements	Reflection mode under grazing or any incidence angle in small-angle range or around any RLN located above the sample surface	
Heating conditions	Heating element	80 at.% platinum–20 at.% rhodium alloy plate
	Maximal temperature	2000 K
	Maximal heating/cooling rate	50 K min^{-1}
	Working pressure	Atmospheric pressure
	Gas flux	Mixing of any two different gases with respect to the conventional security rules A few millilitres per minute to one litre per minute
Bulk single-crystalline or polycrystalline samples	Typical size of the surface	10 × 10 mm
	Typical sample thickness	A few tenths of a millimetre to a few millimetres
Powdered samples	The powder is located in a counterbore (0.5 mm depth and 12.5 mm diameter) machined on a sapphire cylindrical piece	
Global dimension of the furnace	Stage diameter	140 mm
	Stage height	96.5 mm with the dome
Confinement around the sample	Beryllium dome	

powder or a bulk sample). We report in Fig. 2 parts of diffraction patterns recorded on the D2AM beamline on a powdered sample made of a mixture of industrial zirconia powder and the NIST SRM 676a alumina powder. The energy of the X-ray beam was fixed at 17.9 keV. Before each diffraction measurement at any temperature, the sample position along the z axis is corrected as explained above. According to Touloukian *et al.* (1977), the temperature of the sample can be determined from the thermal expansion coefficients along the a and c axes of alumina. The main diffraction peaks observed in the patterns are those of both monoclinic and tetragonal zirconia. Zooming with respect to the q axis between 17.5 and 18.5 nm^{-1} evidences the displacement of the 012 diffraction peak of alumina with respect to the increase of the temperature. Of course, increasing the temperature induces a decrease of the q value of the peak position. At higher temperature, this position is roughly equal to 17.755 nm^{-1}. According to Touloukian *et al.* (1977), this corresponds to 2090 K and this is the higher sample temperature that we reached. We nevertheless fix the maximal working temperature of the QMAX furnace to 2000 K (see Table 1).

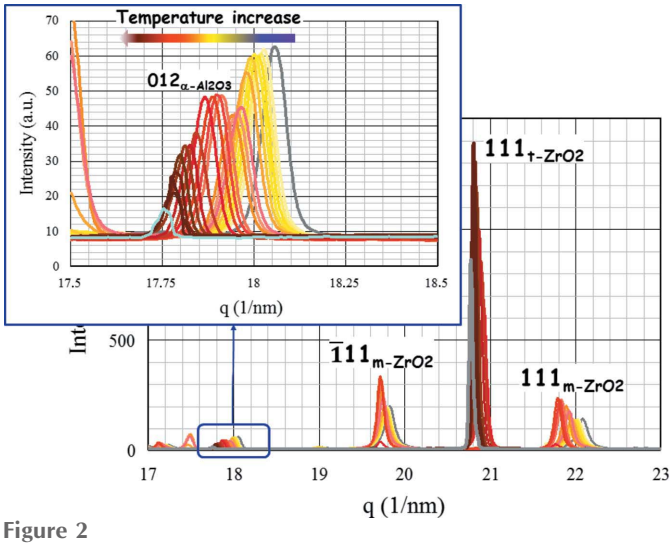

Figure 2
Thermal expansion of α-alumina in a zirconia–alumina powder mixture. The lower Q position of the 012 diffraction peak corresponds to a temperature of 2100 K.

In the following sections, we will present different cases of *in situ* high-temperature studies realized on the D2AM beamline at the ESRF using the QMAX furnace described above. Both the scientific topics that are concerned and the types of samples studied were very different. The first case addresses the self-organization processes on single-crystal vicinal surfaces. The second study illustrates the capability of the setup to follow thermal expansion and to show phase transitions and crystal growth in a crystalline powder as a function of the temperature or during isothermal treatment. The third case concerns a similar approach on bulk polycrystalline samples. It shows the relationship between phase transition and residual stress relaxation processes. In the last example, we illustrate the capability of our setup to follow the oxidation process of metallic plates during a rapid increase of the temperature (20 K min^{-1}). In all cases, the experimental results that we present are not discussed from the point of view of their meaning with respect to materials science. Such discussions are out of the scope of this article and they will be presented in forthcoming papers.

3. 3D grazing-incidence small-angle X-ray scattering at high temperature on vicinal single-crystal surfaces

Thermal treatment of vicinal surfaces of single crystals usually induces step bunching that results in the formation, through a self-organization process, of periodic hill-and-valley structures at the mesoscopic scale (Misbah *et al.*, 2010). These ordered surfaces can be very well imaged through near-field microscopy observations. Nevertheless, such local observations probe micrometric areas, and more global characterization methods such as GISAXS are also mandatory.

Sapphire, *i.e.* α-alumina single crystals, is commonly used as a substrate for the growth of various oxide nanostructures used in light-emitting diodes (Nakamura, 1998; Koester *et al.*,

2011), zinc oxide nanodots and nanowires for electroluminescent devices (Huang *et al.*, 2001; Eaton *et al.*, 2016), as well as lithium niobate epitaxial thin films for electro-optical modulators (Boulle *et al.*, 2009). It has been shown that the use of sapphire vicinal substrates allows controlling the growth process and the size or the shape of the dots grown onto such surfaces (Lee, 2007; Ago *et al.*, 2007; Bachelet, Cottrino *et al.*, 2007; Bachelet, Boulle *et al.*, 2007; Camelio *et al.*, 2007). The crystallographic structure of sapphire is described in the trigonal $R\bar{3}c$ space group and it is usually represented in the hexagonal multiple cell. Throughout this paper, indexings will be given with respect to this hexagonal setting.

A few years ago, we demonstrated that thermal treatment of sapphire vicinal surfaces obtained by cutting single crystals with a miscut angle of 10° with respect to the (006) planes allows promoting the formation of well ordered surfaces exhibiting periodic steps with a width of a few tens of nanometres, depending on the temperature, the duration and the atmosphere of the thermal treatment (Thune *et al.*, 2017; Matringe *et al.*, 2017). However, a significant ordering effect is observed only when the thermal treatment is realized at temperatures higher than 1250 K in air or oxygen-rich atmospheres. In addition, one of the most remarkable results achieved in these studies is the observation of 1D as well as 2D ordered surfaces (Matringe, 2016). The previous investigations left open the question of whether the 2D structure appears by a rearrangement of the 1D structure or these two structures are alternatives to one another. Answering this question requires certainty that the observed area of the sample is always the same for each thermal treatment condition; this is very difficult to achieve through *ex situ* measurements, as it would require that a set of samples that are initially strictly identical is used. We have thus made use of the new QMAX furnace to follow the self-ordering process through *in situ* GISAXS measurements performed under isothermal conditions. However, observation of significant evolution for a reasonable amount of time (*i.e.* a few hours) compatible with the availability of the synchrotron beamtime requires the achievement of measurements at at least 1450 K under pure oxygen continuous flux. While each GISAXS map corresponds roughly to a (q_y, q_z) 2D slice of the reciprocal space, 3D measurements are obtained by recording a large set of (q_y, q_z) maps at different azimuthal angles (around the φ axis). The intensity distribution collected through GISAXS 2D measurements is very sensitive to the z position of the sample and to the angle of incidence of the primary X-ray beam onto the studied surface. It is therefore very important that these two parameters are kept constant throughout the 3D measurement, with an accuracy of 10 µm and 0.01°, respectively.

We followed continuously the self-organization process of a sapphire vicinal surface during isothermal treatment at 1600 K under pure oxygen flux for a period of 40 h. The GISAXS signal was recorded at 8 keV with an incidence angle of 0.30° and using version 3.2 of the XPAD 2D hybrid pixel detector (Medjoubi *et al.*, 2010; Le Bourlot *et al.*, 2012) located at 5050 mm from the sample. The surface was elaborated with a miscut angle equal to 10° with respect to the (006) sapphire planes and in such a way that the step edges were parallel to the $[1\bar{1}0]$ direction. The azimuthal orientation was determined from the diffraction of the (1 1 12) planes and the zero value of the φ rotation was defined as the position where these planes were in the diffraction condition, *i.e.* with the primary beam orthogonal to the [110] direction. Because the $[1\bar{1}0]$ direction of sapphire is orthogonal to [110], in this situation the step edges are strictly parallel to the primary X-ray beam. After convenient alignment, we were able to record 3D RSMs composed of 721 (q_y, q_z) 2D maps collected with a 0.5° rotation step around the φ axis. A full 3D RSM was obtained with a good signal-to-noise ratio in only 15 min. Because significant evolution of the surface took several hours, we can consider that time-resolved measurements were thus carried out.

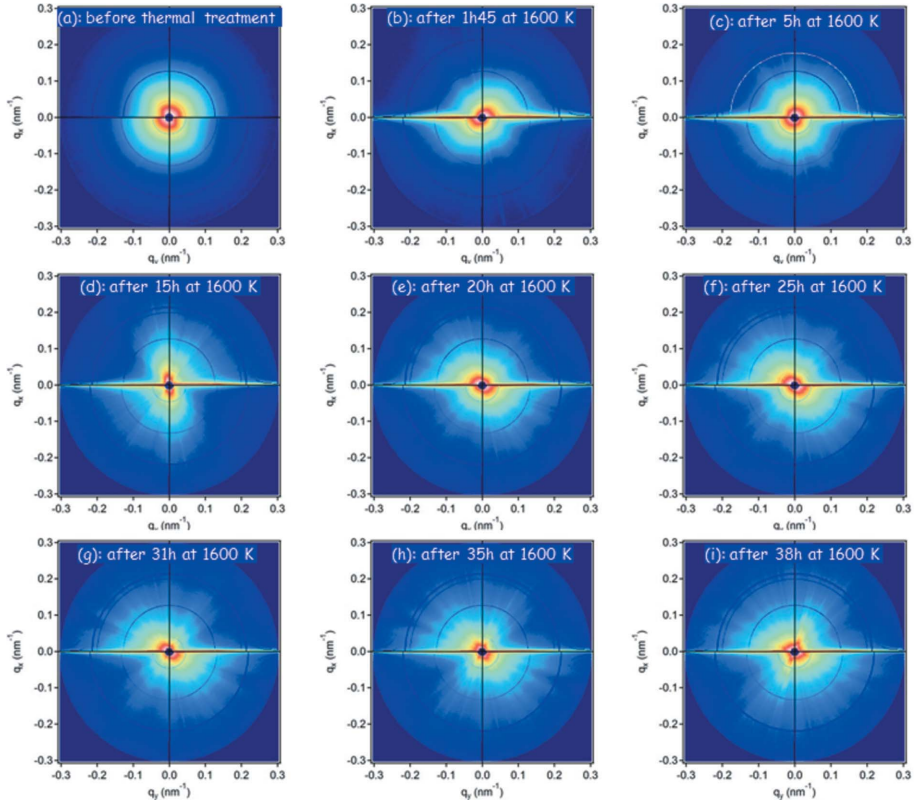

Figure 3
Self-organization of a sapphire vicinal surface during 40 h of isothermal treatment at 1600 K and atmospheric pressure under pure oxygen flux.

During the temperature increase, because of the thermal expansion not only of the sample but also of some parts of the heating sample holder, the sample surface shifts and can be more or less disoriented. As mentioned above, the entire furnace is located on top of the goniometer head, and therefore the correct height and the orientation of the sample can be recovered at any temperature. After the target temperature had been reached, the sample surface was thus fully realigned. Furthermore, the true temperature of the sample was determined according to the thermal expansion law of the c cell parameter of sapphire (Touloukian *et al.*, 1977) through measurement of the position of the 0, 0, 6 sapphire RLN. It is noticeable that no shift or twist of the sample was observed during the roughly two days of isothermal treatment at 1600 K.

Projections along the q_z axis of some of the obtained 3D RSMs are reported in Fig. 3. Before any thermal treatment, the vicinal surface is composed of steps without any order and the scattering signal reported in Fig. 3(*a*) is isotropic. After 1 h 45 min, the projection of the 3D RSM exhibits very clearly a scattering line along the q_y direction which, according to the sample orientation, is due to the ordering of the steps. This scattering line is observed throughout the thermal treatment. Additional structures in the scattered signal progressively appear in the maps recorded after more than 5 h, with specific diffuse scattering lines being observed. According to *ex situ* GISAXS measurements (Matringe, 2016; Matringe *et al.*, 2020), the presence of these diffuse scattering lines is related to the appearance of the 2D ordering.

We demonstrated with this experiment that, thanks to the QMAX furnace, 3D GISAXS signals can be recorded *in situ* over a few tens of hours at very high temperatures under a controlled atmosphere.

4. Thermal expansion, phase transitions and crystal growth in crystalline powders

In the previous example, the sample was a single crystal and the true temperature was determined via measurement of the position of one of the RLNs of the sample itself. Of course, such an approach is more difficult to implement for the characterization of powdered samples. We thus constructed a (006)-oriented single-crystalline sample holder made of a cylindrical piece of sapphire in which we machined a 0.5 mm-deep counterbore that can be filled by the sample powder. A small dot of sapphire is preserved in the center of this sample holder [see Fig. 4(*a*)]. At each set-point temperature, the true temperature can be determined through the measurement of the positions of the 0, 0, 6 and 0, 0, 12 RLNs of sapphire. A typical illustration of the discrepancy between the target temperature and the measured one is reported in Fig. 4(*b*) in the range between 400 and 2000 K. At low temperature, the sample temperature is higher than the set-point one. This gap is certainly related to the use of a Pt–10% Rh–Pt thermocouple that is not very efficient below 700 K. Between 700 and 1400 K the temperatures of the thermocouple and of the sample are close to each other and a higher gap is observed for higher temperature. The maximal gap between the target and the measured value is roughly 60 K. This observation fully illustrates the relevance of a direct measurement of the actual sample temperature, which is the only one that is really interesting from the material characterization point of view.

Besides its ability to allow the determination of the sample temperature, the use of this single-crystalline sample holder presents other interesting features. First of all, the procedure that we described to define with a very high accuracy the orientation of a single-crystalline sample (Section 3) can be used for powdered samples. Such an accurate positioning of powdered samples can be of interest when rotation around the azimuthal axis is used or when the instrumental function needs to be optimized for high-resolution XRD measurements devoted to quantitative microstructural studies. The second important feature

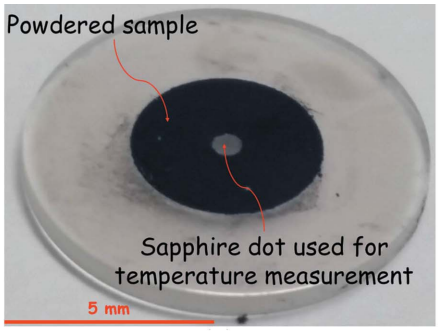

(*a*)

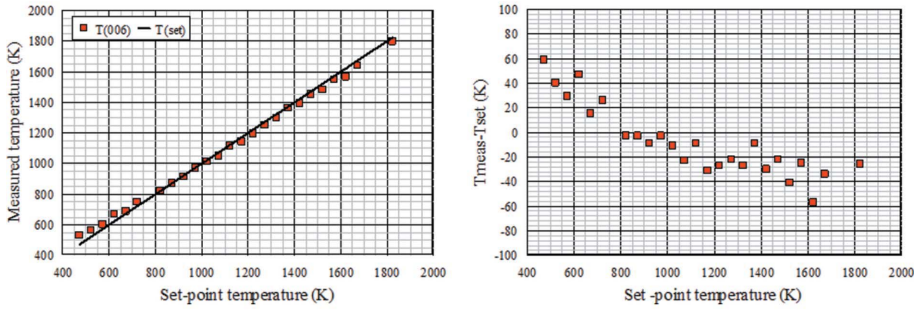

(*b*)

Figure 4
Sample holder for powders and measurement of the sample temperature. (*a*) The powder sample holder. (*b*) Evolution of the temperature determined with respect to the position of the sapphire 0, 0, 6 RLN as a function of the set-point temperature, and evolution of the discrepancy between the measured and set-point temperatures.

concerns the probed volume. For a number of reasons, XRD experiments realized at synchrotron radiation sources are often done using high-energy X-ray beams. The penetration depth is thus often several hundreds of micrometres or higher. The use of a single-crystalline sample holder allows the thickness of the probed volume to be strictly defined and thus the line broadening due to the sample transparency to be limited (Misture *et al.*, 1994).

Zirconium oxide, *i.e.* zirconia, has been used for more than five decades in a very large number of applications, including high-quality brick for glass furnaces, ceramic materials exhibiting wide-ranging mechanical properties, thermal barrier coatings for aircraft, solid-state ionic conductors for oxide fuel cells and basic compounds of biomedical implants. In most cases, the production of zirconia materials requires the use of high or very high temperatures and, in a large number of applications, these materials are used at high temperature. Knowledge of the thermal behavior of zirconia is thus essential. Under atmospheric pressure, pure zirconia (ZrO_2) exhibits two solid-state phase transitions (SPTs) during cooling from the liquidus temperature. It solidifies into a cubic crystal structure ($Fm\bar{3}m$ space group) at about 3000 K, transforms to tetragonal (t) ($P4_2/nmc$ space group) upon cooling to 2575 K and becomes monoclinic (m) ($P2_1/c$ space group) at 1440 K (Smirnov *et al.*, 2003). Because of the values of the temperatures under consideration, it is a hard task to obtain accurate experimental data on the SPT processes. As indicated above, tetragonal zirconia crystallized in the primitive $P4_2/nmc$ space group. Nevertheless, this structure is commonly described in terms of the pseudo-cubic 'face-centered tetragonal' lattice in which the crystallographic directions are parallel to those of the cubic form [see for example Kisi (1998)]. This setting is very efficient in terms of following the m ↔ t phase-transition process. Accordingly, we adopt it in this paper.

Hill & Cranswick (1994) reported a round-robin test on the structure refinement through X-ray and neutron diffraction of powdered samples and the Rietveld method. This study was realized under the auspices of the International Union of Crystallography and two different samples were used. One of them was a powder of monoclinic zirconia synthesized by the wet chemical route (referred to below as the 'IUCr sample'), and we have recently used a small amount of it to show the capability of the QMAX furnace concerning XRD on powdered samples.

High-temperature XRD patterns were recorded at 17.6 keV using a 2D hybrid pixel detector (XPAD) located at 800 mm from the sample on the goniometer 2θ arm. We followed the structural evolution of the powder between RT and 1800 K. At each temperature, 21 images were recorded in $\theta-2\theta$ mode using a 1° 2θ step between 8 and 28°. Only 5 s were needed for recording one image and the total signal was thus obtained in less than 2 min. The 21 2D images were merged and integrated using a special class (multi-geometry) of the *pyFAI* library (Ashiotis *et al.*, 2015) to reconstruct 1D diffraction patterns. The part of the reciprocal space explored was between 12 and 55 nm^{-1}, which contains all the significant diffraction peaks of the different zirconia phases.

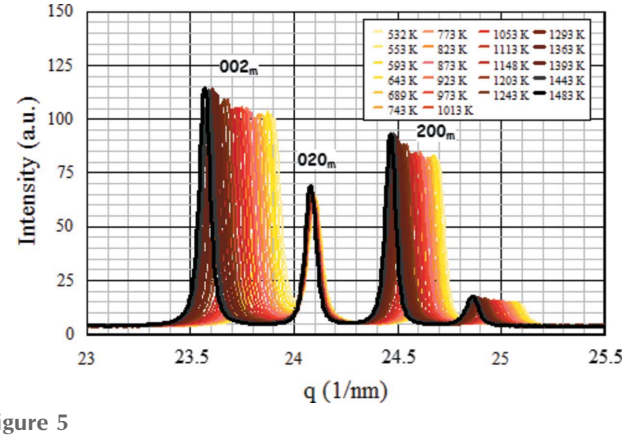

Figure 5
Anisotropy of the thermal expansion of monoclinic zirconia.

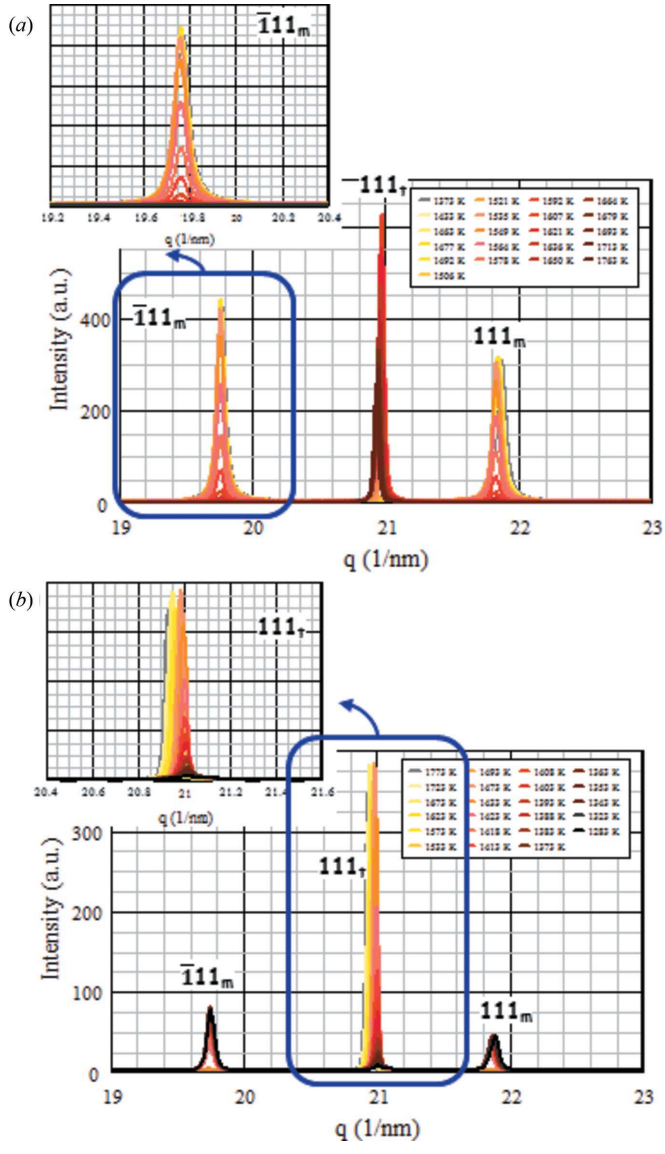

Figure 6
In situ observation between 1350 and 1800 K of the tetragonal ↔ monoclinic phase transition in the IUCr pure zirconia powder during (*a*) the increase and (*b*) the decrease of the temperature.

A part of the patterns recorded between RT and 1500 K is reported in Fig. 5. This figure is a very clear illustration of the strong anisotropy of the thermal expansion of monoclinic zirconia. The expansion along the **a** and **c** cell vectors is very significant. Simultaneously, the β angle decreases (not shown here). Conversely, the b cell parameter is almost constant, whatever the temperature. The discussion of this observation is out of the scope of this article; nevertheless, it can be noted that such an anisotropy will generate in zirconia-based bulk materials large and anisotropic residual stresses.

Thermal treatment at higher temperature induces the monoclinic to tetragonal SPT and the reverse process during cooling. XRD patterns were recorded every 10 K or even 5 K between 800 and 1800 K. Some of these patterns illustrating the SPTs are reported in Fig. 6. The m $\rightarrow$ t transition starts at around 1450 K, and at 1630 K all the crystals have tetragonal symmetry. The reverse transition, t $\rightarrow$ m, starts close to 1450 K and ends below 1150 K. We show here that even in this powdered sample, *a priori* free of any internal stresses, the phase-transition process extends over more than 200 K. The t $\leftrightarrow$ m phase transition in zirconia is a first-order transition and it is of martensitic type. According to Hill (1992), the mean size of the zirconia crystals in the pristine sample is 62 nm. The temperature spread of the phase transition and the thermal hysteresis are related to size and microstrain effects that we will not discuss here.

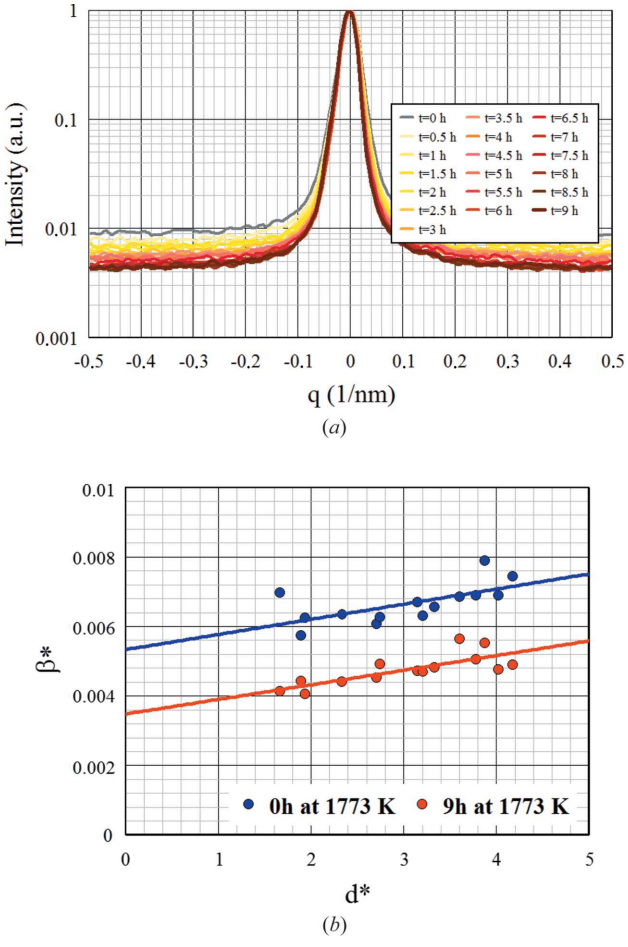

Figure 7
In situ study of the tetragonal zirconia crystal growth in the IUCr pure zirconia powder during a 9 h isotherm at 1773 K. (*a*) Evolution of the profile of the 111 tetragonal diffraction peak during the isothermal treatment. (*b*) Williamson–Hall plot.

Since Scherrer's pioneering work (Scherrer, 1918), it has been well known that line-profile analysis of the XRD peaks is an efficient method for quantitatively determining the main microstructural parameters of powdered or bulk nanostructured polycrystalline materials. Very often, the microstructural evolution is not reversible and it is thus important to catch processes such as crystal growth, microstrain relaxation, and variation of the density of stacking faults or dislocations *in situ*. We studied the microstructural evolution of the IUCr zirconia sample during a 9 h isothermal treatment at 1773 K under airflow. As mentioned above, each full pattern is recorded in less than 2 min. Such measurements will allow one to extract with high accuracy the kinetics of crystal growth, and this will be presented in a forthcoming paper. The isothermal evolution at 1773 K of the 111 tetragonal zirconia peak is reported in Fig. 7(*a*), where one pattern taken every half an hour is shown. The diffracted intensity is normalized and reported in log scale. We observed throughout the isothermal treatment a clear condensation of the diffuse scattering. The peak narrows in width and its profile evolves with a decrease of its Lorentzian part.

As a preliminary result, a Voigt function was used to fit the diffraction peaks of the first and the last patterns recorded during the isothermal treatment. Following the Williamson–Hall approach (Williamson & Hall, 1953), we plotted the evolution of $\beta^* = \beta \cos\theta/\lambda$ (where β is the full width at half-maximum of the diffraction peaks) as a function of the reciprocal-space vector length d^* [see Fig. 7(*b*)]. According to the y intercepts of the straight lines, the mean size of the tetragonal crystals evolves from 190 to 290 nm during the whole isotherm at 1773 K. Moreover, when looking at the slopes of the corresponding linear fits, it seems that the amount of microstrain stays roughly constant during the isothermal treatment.

5. Phase transitions and diffuse scattering into bulk polycrystalline samples

The physical properties of bulk metallic alloys and ceramic materials are often significantly different from those of the powders of the same compounds. In fact, residual stresses appearing during the synthesis of bulk materials through fused cast or sintering processes very often have a strong influence on the behavior of the materials under external constraints. The ability to determine the structural and microstructural evolution *in situ* in bulk samples is thus often a key point for the development of new objects or devices. The QMAX furnace was built in such a way that it allows the characterization of bulk polycrystalline samples under conditions similar to those used for powdered samples. Samples exhibiting a typical surface of 1 cm^2 and a thickness of 1 mm can be put on top of the furnace, glued or not on a ceramic coating deposited on the heating element. For the first two examples,

the sample temperature was determined through the measurement of the thermal expansion α-alumina. However, we used powder instead of a single crystal. Before the experiment, a thin layer of NIST SRM 676a alumina powder was spread onto the bulk samples' surface and we determined the sample temperature according to the thermal evolution of the a and c cell parameters of α-alumina.

As an illustration of high-temperature *in situ* XRD experiments on polycrystalline bulk samples, we studied dense ceramic samples that are part of large zirconia blocks elaborated through a specific fused cast process developed by the St Gobain company in order to manufacture large bricks (submetre scale) used as refractory components in industrial furnaces devoted to the production of glass. The sample was composed of sub-millimetre zirconia dendrites embedded into a silica-based glassy phase and it contains 95% pure zirconia. More details about the microstructure of this material have been published elsewhere (Patapy *et al.*, 2013). The XRD patterns were collected at 17.9 keV, just below the zirconium absorption edge, using the same 2D hybrid pixel detector as for the experiments on powdered samples (see previous section). Taking into account both the energy and the incidence angle of the X-ray beam, the penetration depth was close to 100 µm. Finally, according to the sub-millimetre size of this beam, the probed volume was in all cases smaller than one dendrite. We have shown previously (Örs *et al.*, 2018) through Laue microdiffraction that each dendrite can be considered to be mechanically independent of the rest of the sample. Moreover, we have demonstrated (Humbert *et al.*, 2010) that all monoclinic crystals constituting at RT one dendrite result in fact from the two successive SPTs (*i.e.* cubic → tetragonal and tetragonal → monoclinic) of one unique initial cubic crystal.

Parts of the Debye–Scherrer rings recorded on such a sample at RT are reported in Fig. 8(*a*). This diffraction pattern shows that the diffracted intensity is located in specific areas along the Debye–Scherrer rings. This feature is due to the crystallographic texture effect induced by the SPTs, and it means that some crystals having a similar crystallographic orientation are diffracting in a specific part of the reciprocal space.

All the crystals diffracting at RT in this part of the reciprocal space correspond to crystals having the same orientation in the tetragonal form. Taking into account this global common orientation, we were able to find another RLN of the same set of monoclinic crystals and to fully determine in three dimensions the global orientation of these crystals. Finally, we have recorded 3D RSMs through *hkl* scans close to the 1, 1, 1 tetragonal RLN as a function of the temperature up to 1473 K. At each considered temperature, 200 2D maps were recorded in roughly 1 h. The 3D maps were reconstructed using a Python routine developed at the D2AM beamline. The evolution of the diffuse scattering signal is illustrated in Fig. 8(*b*).

According to the loss of the threefold symmetry of the cubic space group around the [*hhh*] axis, each monoclinic node is in fact split into three different maxima. At 1373 K a large part of the zirconia crystals have the tetragonal form and the diffuse scattering has almost disappeared. Decreasing the temperature induces reappearance of a weaker diffuse scattering signal. This feature is clearly due to a coupling between strain

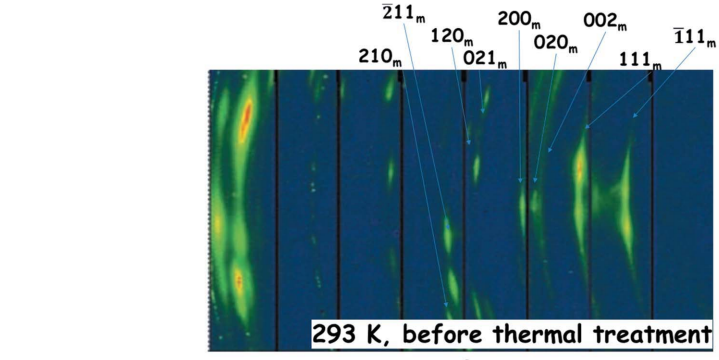

(*a*)

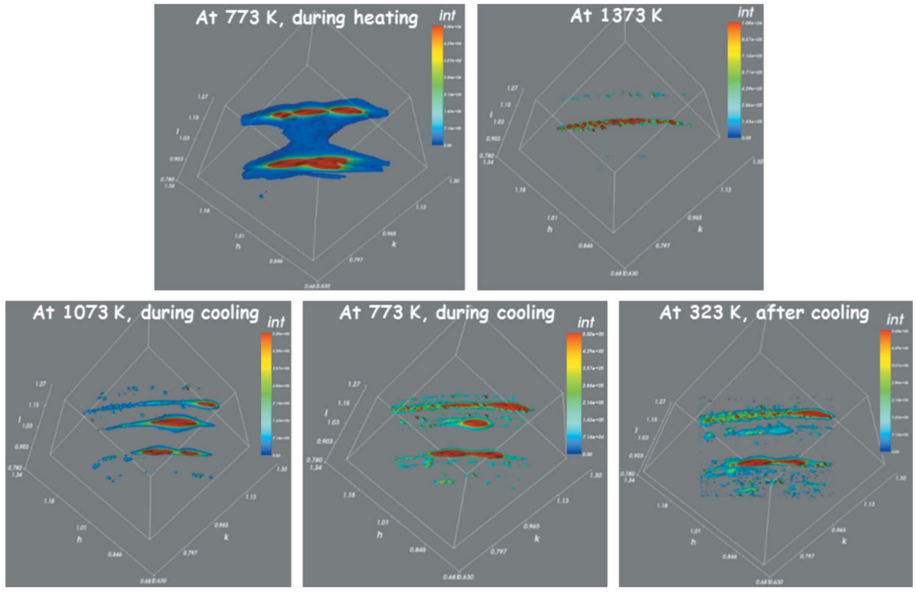

(*b*)

Figure 8
Phase transitions, diffuse scattering and stress relaxation at high temperature in a bulk zirconia ceramic sample. (*a*) Part of Debye–Scherrer rings diffracted by one zirconia dendrite. (*b*) 3D reciprocal space maps around the $\bar{1}$, 1, 1 and 1, 1, 1 monoclinic RLNs at high temperature.

relaxation and the t ↔ m phase transition. The volume of the monoclinic cell is roughly 4% higher than that of the tetragonal cell, and therefore, during heating, the m → t transition is associated with stress relaxation. Conversely, the reverse t → m transition induces the appearance of huge stresses that are partially relaxed by the formation of a microcrack network around the monoclinic crystals (Kisi, 1998). Detailed description of this feature and of the interdependency of size and strain effects requires micromechanical modeling and is far from the topic of this paper. Nevertheless, we have shown here that using the QMAX furnace the coupled strain and diffuse scattering evolution on polycrystalline samples can be captured *in situ* at high temperature.

6. *In situ* oxidation of metals under controlled atmosphere

In all the experimental cases presented above, the measurements were done under air or oxygen flux, and because the studied samples were oxides, no chemical reaction between the sample and the surrounding atmosphere was expected. As a last illustration of the capabilities of the QMAX furnace, we present an *in situ* reactive high-temperature time-resolved experiment. The samples were flat plates of zirconium alloy and the general aim of the study was to understand the oxidation of this metallic alloy submitted to quick variations of the temperature up to 1450 K under oxygen-rich atmosphere. According to the literature, in the range from 975 to 1450 K, the kinetics of the oxidation process of zirconium alloy strongly depend on the temperature. Very fast processes are expected at high temperature and our aim was to follow the formation of the oxide with a time resolution of about 1 min during heating and 1 s during isothermal treatment. All of the diffraction patterns were recorded using a large 2D hybrid pixel detector (XPAD-WOS) available at the beamline and allowing a large part of the Debye–Scherrer rings to be recorded without any detector movement. This detector was fixed on the 2θ goniometer arm and the energy of the X-ray beam was fixed at 17.6 keV. The position of the detector was fixed at 850 mm from the specimen in such a way that, according to the energy of the X-ray beam, the oxide diffraction main peaks are clearly visible between the main diffraction peaks of the zirconium alloy [see Fig. 9(*a*)].

Because of the kinetics of the oxidation process, measurement of the sample temperature was not straightforward. It was monitored via two thermocouples, one fixed on the heating resistor and one spot-welded directly on the specimen surface. Accurate temperature was also determined by following the evolution of the cell parameters of the NIST SRM 676a alumina powder placed on top of the sample.

The main stumbling block with respect to the realization of reactive experiments able to capture structural evolution of samples lies in the control of the gas atmosphere. Using the two gas lines linked to the furnace (see Section 2), we were able to monitor the composition of a helium–oxygen gas mixture as a function of time and temperature through a computer-controlled process. As illustration, we report in Fig. 9(*b*) the evolution of the diffraction patterns evidencing the oxidation of zirconium during heating from RT to 1050 K at a rate of 20 K min^{-1} and under a 1000 ml min^{-1} flux of 90%He–10%O_2 gas mixture. Patterns were recorded every 30 s. For clarity, below 773 K, only a few patterns are reported in Fig. 9(*b*). At higher temperatures, half of the recorded patterns are shown, which thus roughly corresponds to temperature steps of 20 K.

One of the aims of the study was to follow the relative amount of monoclinic and tetragonal zirconia appearing under oxidation atmosphere. The zirconia crystals have a size between a few nanometres and a few tens of nanometres, and

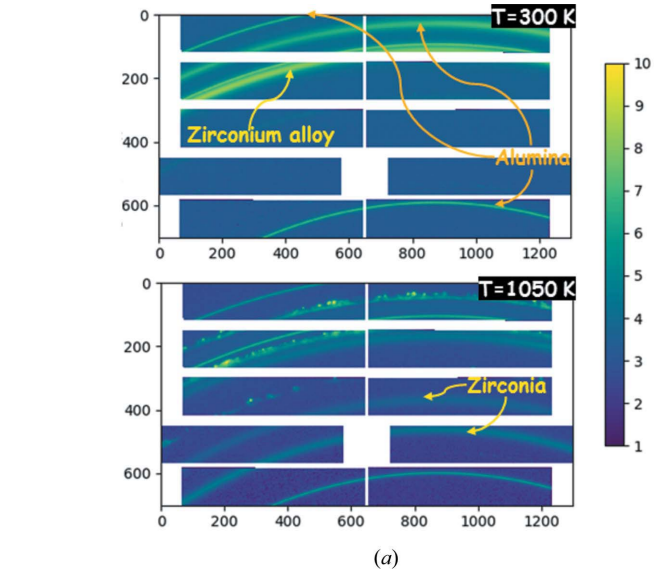

(*a*)

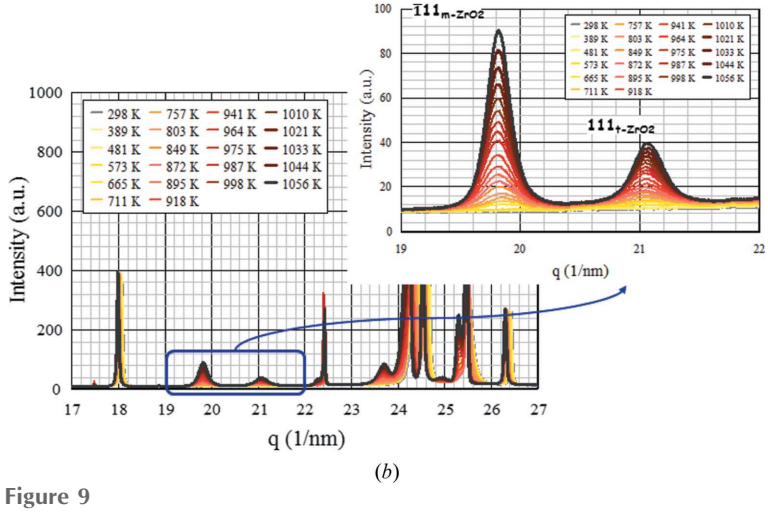

(*b*)

Figure 9
Oxidation of a zirconium-based alloy at high temperature under the controlled atmosphere of an He–O_2 reactive gas mixture. (*a*) Part of the Debye–Scherrer rings observed at RT and close to 1050 K. Two different rings corresponding to the diffraction by zirconia crystals are clearly visible at high temperature. (*b*) Evolution of the XRD patterns during heating at 20 K min^{-1} between RT and 1100 K.

the relative amounts of tetragonal and monoclinic phases are strongly related to the size of these nanocrystals. We were able to follow the evolution of the mean size of both tetragonal and monoclinic zirconia crystals through line-profile analysis during isothermal treatment realized at different temperatures between 973 and 1273 K with a time scale of 10 s.

7. Concluding remarks

We have built, through a 5 year collaborating research program funded by the ANR (ANR-09-NANO-031), a unique high-temperature furnace implemented at the D2AM beamline at the ESRF. X-ray scattering or diffraction measurements can be carried out at up to 2000 K under controlled gas flux at atmospheric pressure under reflection geometry. We have shown with the above description of four very different cases that this QMAX furnace is well adapted for GISAXS and GID experiments as well as asymmetric and symmetric XRD on powdered and bulk samples under inert and reactive gas mixtures. The combination of the QMAX furnace and state-of-the-art 2D hybrid pixel detectors allows the full exploration of the reciprocal space everywhere above the sample plane.

Owing to the presence of a high-precision motorized goniometer head on top of the D2AM kappa diffractometer, the translational and angular positions of the samples can be precisely adjusted as a function of temperature, and at any temperature, with an accuracy of a few tens of micrometres and a few hundredths of a degree. We have also shown that we were able to maintain this high-precision positioning for a period of two days at a temperature as high as 1600 K.

The development of devices based on nanostructured materials requires the ability to follow the evolution of their microstructure during the elaboration process or *operando*. Nowadays, it is clear that *in situ* or *operando* X-ray scattering setups have to be built using a 2D, or at least a 1D, position-sensitive detector. Although a lot of work is currently being done to obtain high angular resolution using 2D position-sensitive detectors [see for example Dejoie *et al.* (2018)], under reflection geometry the resolution remains directly linked to the beam size. We demonstrate that, as a result of the high flux provided by the synchrotron radiation source and in spite of the use of a highly collimated parallel primary X-ray beam, high-resolution XRD patterns can be recorded on a timescale of seconds and full 3D RSMs can be obtained in a few minutes. Such a timescale is very well suited for a large part of the X-ray scattering measurements needed in the field of materials science. These results open up the field of experiments devoted to the *in situ* determination of the microstructure evolution of nanostructured materials at high temperature. We have shown that the study of nanocrystal growth can be performed at 1775 K on the IUCr zirconia standard sample, and we observed relaxation of residual stresses in bulk ceramic materials through a high-temperature phase transition.

External constraints can be imposed by the temperature and the evolution of the atmosphere surrounding the samples. The QMAX furnace has been designed to work under atmospheric pressure. It is thus easy to realize any type of X-ray scattering measurements at high temperature under controlled flux of gas mixture. The chemical reactions between single crystals as well as powdered or bulk polycrystalline samples with various types of gas mixture can thus be followed during isothermal treatments or during high-speed heating or cooling.

Acknowledgements

We acknowledge the ESRF and the French Collaborating Research Group (F-CRG) for provision of synchrotron radiation facility beamtime. H. Song is thanked for his work on the preliminary thermomechanical calculations and the general sizing of the furnace. The building of the furnace has been realized under the technical supervision of D. de Barros. The experiments on the sapphire vicinal surfaces and on the IUCr zirconia powder were realized with the valuable help of C. Matringe (IRCER) and J. B. Marijon (PIMM), respectively. The authors are thankful to I. Cabodi and O. Bories (Saint-Gobain CREE) for the supply of the bulk-zirconia-based materials. M. Huger and F. Gouraud from the IRCER laboratory and T. Örs and V. Michel from the PIMM laboratory are strongly thanked for their involvement during these experiments. The oxidation experiments were realized in the frame of a research program funded by the CEA Paris–Saclay Centre in collaboration with R. Guillou, M. Lesaux, D. Menut and J. L. Bechade, who are also gratefully acknowledged.

Funding information

The QMAX furnace has been designed and built as part of the QMAX Project No. ANR-09-NANO-031 funded by the French National Research Agency (ANR). Experiments on the bulk-zirconia-based samples were done in the frame of the ASZTECH research program funded by the ANR (ANR-12-RMNP-0007).

References

Ago, H., Imamoto, K., Ishigami, N., Ohdo, R., Ikeda, K. I. & Tsuji, M. (2007). *Appl. Phys. Lett.* **90**, 133112.

Ashiotis, G., Deschildre, A., Nawaz, Z., Wright, J. P., Karkoulis, D., Picca, F. E. & Kieffer, J. (2015). *J. Appl. Cryst.* **48**, 510–519.

Bachelet, R., Boulle, A., Soulestin, B., Rossignol, F., Guinebretière, R. & Dauger, A. (2007). *Thin Solid Films*, **515**, 7080–7085.

Bachelet, R., Cottrino, S., Nahélou, G., Coudert, V., Boulle, A., Soulestin, B., Rossignol, F., Guinebretière, R. & Dauger, A. (2007). *Nanotechnology*, **18**, 015301.

Basolo, S., Bérar, J.-F., Boudet, N., Breugnon, P., Caillot, B., Clemens, J.-C., Delpierre, P., Dinkespiler, B., Hustache, S., Koudobine, I., Meessen, C., Menouni, M., Mouget, C., Palancher, H., Pangaud, P., Potheau, R. & Vigeolas, E. (2007). *J. Synchrotron Rad.* **14**, 151–157.

Beck, M. & Mittemeijer, E. J. (2002). *J. Appl. Cryst.* **35**, 103–107.

Bénard, P., Auffrédic, J. P. & Louër, D. (1996). *Mater. Sci. Forum*, **228–231**, 325–334.

Bergamaschi, A., Cervellino, A., Dinapoli, R., Gozzo, F., Henrich, B., Johnson, I., Kraft, P., Mozzanica, A., Schmitt, B. & Shi, X. (2010). *J. Synchrotron Rad.* **17**, 653–668.

Boulle, A., Kilburger, S., Di Bin, P., Millon, E., Di Bin, C., Guinebretière, R. & Bessaudou, A. (2009). *J. Phys. D Appl. Phys.* **42**, 145403.

Boulle, A., Masson, O., Guinebretière, R. & Dauger, A. (2001). *Appl. Surf. Sci.* **180**, 322–327.

Brown, N. E., Swapp, S. M., Bennett, C. L. & Navrotsky, A. (1993). *J. Appl. Cryst.* **26**, 77–81.

Camelio, S., Babonneau, D., Lantiat, D. & Simonot, L. (2007). *Europhys. Lett.* **79**, 47002.

Chahine, G. A., Blanc, N., Arnaud, S., De Geuser, F., Guinebretière, R. & Boudet, N. (2019). *Metals*, **9**, 352.

Cornelius, T. W., Davydok, A., Jacques, V. L. R., Grifone, R., Schülli, T., Richard, M.-I., Beutier, G., Verdier, M., Metzger, T. H., Pietsch, U. & Thomas, O. (2012). *J. Synchrotron Rad.* **19**, 688–694.

Dejoie, C., Coduri, M., Petitdemange, S., Giacobbe, C., Covacci, E., Grimaldi, O., Autran, P.-O., Mogodi, M. W., Šišak Jung, D. & Fitch, A. N. (2018). *J. Appl. Cryst.* **51**, 1721–1733.

Eaton, S. W., Fu, A., Wong, A. B., Ning, C. Z. & Yang, P. D. (2016). *Nat. Rev. Mater.* **1**, 16028.

Estermann, M., Reifler, H., Steurer, W., Filser, F., Kocher, P. & Gauckler, L. J. (1999). *J. Appl. Cryst.* **32**, 833–836.

Gualtieri, A. F., Mazzucato, E., Venturelli, P., Viani, A., Zannini, P. & Petras, L. (1999). *J. Appl. Cryst.* **32**, 808–813.

Guinebretière, R. (2007). *X-ray Diffraction on Polycrystalline Materials*. London: ISTE Ltd.

Guinebretière, R., Boulle, A., Bachelet, R., Masson, O. & Thomas, P. (2007). *J. Appl. Cryst.* **40**, 332–337.

Hill, R. J. (1992). *J. Appl. Cryst.* **25**, 589–610.

Hill, R. J. & Cranswick, L. M. D. (1994). *J. Appl. Cryst.* **27**, 802–844.

Huang, M. H., Mao, S., Feick, H., Yan, H. Q., Wu, Y. Y., Kind, H., Weber, E., Russo, R. & Yang, P. D. (2001). *Science*, **292**, 1897–1899.

Humbert, M., Gey, N., Patapy, C., Joussein, E., Huger, M., Guinebretière, R., Chotard, T. & Hazotte, A. (2010). *Scr. Mater.* **63**, 411–414.

Kisi, E. (1998). *Zirconia Engineering Ceramics. Old Challenges – New Ideas*. Zürich: Trans Tech Publications.

Koester, R., Hwang, J. S., Salomon, D., Chen, X., Bougerol, C., Barnes, J. P., Dang, D. L. S., Rigutti, L., Bugallo, A. L., Jacopin, G., Tchernycheva, M., Durand, C. & Eymery, J. (2011). *Nano Lett.* **11**, 43839–43845.

Koppelhuber-Bitschnau, B., Mautner, F. A., Worsch, P. & Gautsch, J. (1996). *Mater. Sci. Forum*, **228–231**, 137–142.

Kotnik, P., Hofbauer, P., Resel, R., Koini, M., Haber, T. & Keckes, J. (2006). *Acta Cryst.* A**62**, s158.

Leake, S. J., Chahine, G. A., Djazouli, H., Zhou, T., Richter, C., Hilhorst, J., Petit, L., Richard, M.-I., Morawe, C., Barrett, R., Zhang, L., Homs-Regojo, R. A., Favre-Nicolin, V., Boesecke, P. & Schülli, T. U. (2019). *J. Synchrotron Rad.* **26**, 571–584.

Le Bourlot, C., Landois, P., Djaziri, S., Renault, P.-O., Le Bourhis, E., Goudeau, P., Pinault, M., Mayne-L'Hermite, M., Bacroix, B., Faurie, D., Castelnau, O., Launois, P. & Rouzière, S. (2012). *J. Appl. Cryst.* **45**, 38–47.

Lee, G. H. (2007). *Mater. Sci. Eng. B*, **138**, 41–45.

Masson, O., Guinebretière, R. & Dauger, A. (1996). *J. Appl. Cryst.* **29**, 540–546.

Matringe, C. (2016). PhD thesis, University of Limoges, France.

Matringe, C., Fakih, A., Thune, E., Babonneau, D., Arnaud, S., Blanc, N., Boudet, N. & Guinebretière, R. (2017). *Appl. Phys. Lett.* **111**, 031601.

Matringe, C., Thune, E., Cavalotti, R., Fakih, A., Arnaud, S., Blanc, N., Boudet, N., Coati, A., Garreau, Y., Babonneau, D. & Guinebretière, R. (2020). *Nano Res.* In the press.

Medjoubi, K., Bucaille, T., Hustache, S., Bérar, J.-F., Boudet, N., Clemens, J.-C., Delpierre, P. & Dinkespiler, B. (2010). *J. Synchrotron Rad.* **17**, 486–495.

Misbah, C., Pierre-Louis, O. & Saito, Y. (2010). *Rev. Mod. Phys.* **82**, 981–1040.

Misture, S. T., Chatfield, L. R. & Snyder, R. L. (1994). *Powder Diffr.* **9**, 172–179.

Misture, S. T., Hubbard, C. R. & Wang, X. L. (2002). *Adv. X-ray Anal.* **45**, 25–30.

Montano, A. & Oyanagi, H. (1999). Editors. *In Situ Synchrotron Radiation Research in Materials Science*, MRS Bulletin, Vol. 24, No. 1. Warrendale: Materials Research Society.

Muller, F., Rannou, I., Duclaux, L. & Guet, J. M. (1997). *J. Appl. Cryst.* **30**, 557–558.

Nakamura, S. (1998). *Science*, **281**, 956–961.

Örs, T., Micha, J.-S., Gey, N., Michel, V., Castelnau, O. & Guinebretiere, R. (2018). *J. Appl. Cryst.* **51**, 55–67.

Patapy, C., Huger, M., Guinebretière, R., Gey, N., Humbert, M., Hazotte, A. & Chotard, T. (2013). *J. Eur. Ceram. Soc.* **33**, 259–268.

Pickup, D. M., Mountjoy, G., Roberts, M. A., Wallidge, G. W., Newport, R. J. & Smith, M. E. (2000). *J. Phys. Condens. Matter*, **12**, 3521–3529.

Sarin, P., Haggerty, R. P., Yoon, W., Knapp, M., Berghaeuser, A., Zschack, P., Karapetrova, E., Yang, N. & Kriven, W. M. (2009). *J. Synchrotron Rad.* **16**, 273–282.

Scherrer, P. (1918). *Nachr. Ges. Wiss. Gott. Math. Phys.* **1–2**, 96–100.

Smirnov, M., Mirgorodsky, A. & Guinebretière, R. (2003). *Phys. Rev. B*, **68**, 104106.

Tao, F. & Salmeron, M. (2011). *Science*, **331**, 171–174.

Thune, E., Fakih, A., Matringe, C., Babonneau, D. & Guinebretière, R. (2017). *J. Appl. Phys.* **121**, 015301.

Touloukian, Y. S., Kirby, R. K., Taylor, R. E. & Lee, T. Y. R. (1977). *Thermophysical Properties of Matter*, Vol. 13, pp. 173–193. New York: Plenum.

Villanova, J., Daudin, R., Lhuissier, P., Jauffrès, D., Lou, S., Martin, C. L., Labouré, S., Tucoulou, R., Martinez-Criado, G. & Salvo, L. (2017). *Mater. Today*, **20**, 354359.

Williamson, G. K. & Hall, W. H. (1953). *Acta Metall.* **1**, 22–31.

Yashima, M. (2002). *J. Am. Ceram. Soc.* **85**, 2925–2930.

Yashima, M., Oh-uchi, K., Tanaka, M. & Ida, T. (2006). *J. Am. Ceram. Soc.* **89**, 1395–1399.

Yashima, M. & Tanaka, M. (2004). *J. Appl. Cryst.* **37**, 786–790.